69th International Astronautical Congress (IAC), Bremen, Germany, 1-5 October 2018.

IAC–18–C1.6.11

Autonomous Small Body Mapping and Spacecraft Navigation

Francesca Baldini[a], **Alexei Harvard**[a], **Soon-Jo Chung**[a], **Issa Nesnas**[b], **and Shyamkumar Bhaskaran**[b]

[a]Graduate Aerospace Laboratories, California Institute of Technology, Pasadena, CA 91125
[b]Jet Propulsion Laboratory, California Institute of Technology, Pasadena, CA 91191
* Corresponding Author

Abstract

Current methods for pose and shape estimation of small bodies, such as comets and asteroids, rely on extensive ground support and significant use of radiometric measurements using the Deep Space Network. The Stereo-Photoclinometry (SPC) technique is currently used to provide detailed topological information about a small body as well as its absolute orientation and position. While this technique has produced very accurate estimates, the core algorithm cannot be run in real-time and requires a team of scientists on the ground who must communicate with the spacecraft in order to oversee SPC operations. Autonomous on-board navigation addresses these limitations by eliminating the need for human oversight. In this paper, we present an optimization-based estimation algorithm for navigation that allows the spacecraft to autonomously approach and maneuver around an unknown small body by mapping its geometric shape, estimating its orientation, and simultaneously determining the trajectory of the center of mass of the small body. We show the effectiveness of the proposed algorithm using simulated data from a previous flight mission to Comet 67P.

Nomenclature

- $p^{\gamma}_{\alpha,\beta}$: position vector from point β to point α expressed with respect to frame γ.
- R^{α}_{β}: rotation matrix from frame β to frame α.
- $J2000$: J2000 Geocentric Earth Equatorial Inertial Frame.
- sb: center of mass of the small body.
- $sb(j)$: small body frame at time j.
- n (superscript or subscript): camera (spacecraft) frame or its origin at time n.
- 0 (superscript or subscript): camera (spacecraft) frame or its origin at time 0.

1 Introduction

The exploration of unknown small bodies requires accurate information of the spacecraft position and attitude in order to achieve successful orbital observations and proximity operations. If we aim to achieve the high precision pose and shape information required for proximity operation and landing, we need to accurately measure the geometric properties of the target small body, for which ground-based observations are not sufficient. The integration of on-board sensor measurements with ground-based observations allows a better characterization of these properties. A major difficulty, when approaching and navigating around an unknown small bodies, arises from the need to estimate the relative position of the spacecraft very precisely while mapping an unknown shape model of the small body without any prior information. The Stereo-Photoclinometry (SPC) technique is currently used to provide topological information about celestial bodies [1, 2, 3]. SPC uses images of the same portion of the small body obtained at different times under different light conditions to estimate the albedo and the slope gradients at each pixel by minimizing the photometric error across all the images. This technique, combined with the spacecraft's locations and camera pointing angles, leads to an iterative optimization-based method of obtaining a detailed shape model of the small body. In order to achieve the topography reconstruction for SPC, hundreds of landmarks maplets (L-maps) are selected manually by scientists and engineers at an optical navigation station on Earth. The centers of each L-maps are particular surface features that are used by the optical navigation technique as control points for

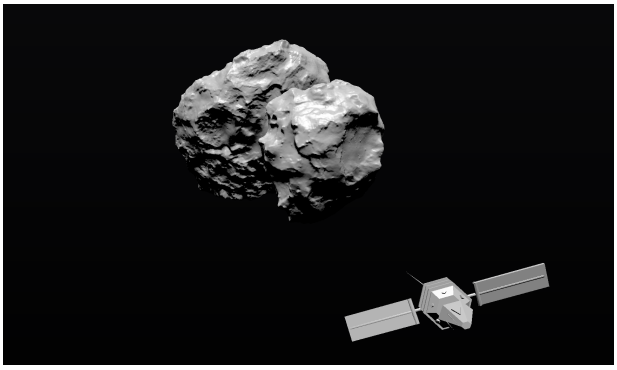

Fig. 1.1: A notional spacecraft model approaching Comet 67P/ Churyumov–Gerasimenko.

the spacecraft navigation [3, 4, 5]. However, this technique requires a large collection of images of the same portion of the small body under different light conditions as well as extensive and time-expensive ground support.

Recently, on-board optical navigation has been studied to achieve autonomous spacecraft localization in additional to automatic landmark recognition [6]. In Autonomous Optical Navigation (AutoNav) [6], the set of functions to perform the spacecraft navigation is transferred from the ground to the spacecraft. Nevertheless, AutoNav requires the landmarks obtained by the SCP technique to perform a complete autonomous on-board navigation. Achieving a completely autonomous navigation technique remains an open research problem for future space missions to small bodies.

If the distance between the spacecraft and the small body exceeds the gravity well of the small body and the operational range of on-board range sensors (e.g., Lidar and radar), only a monocular camera system can be used to get information about the target small body. Simultaneous Localization and Mapping (SLAM) or Structure from Motion (SfM) algorithms using a single monocular camera cannot produce true scale information on its pose and shape estimates, so additional external measurements have to be integrated [7, 8]. In contrast with aerial vehicles, during long-distance operations in space, accelerometer measurements on on-board spacecraft cannot be used to aid in spacecraft state estimation due to relatively constant-velocity motions and noise generated by thrusters. A better approach would be incorporating the high-fidelity dynamic models that capture the gravitational forces between the small body and the spacecraft. A laser altimeter has a limited operating range and so it cannot be used as an initial navigation sensor to determine the position of the spacecraft. Traditional approaches make use of radiometric tracking measurements from Earth. In this paper, it is assumed that such measurements are available. Characteristic feature points can be selected automatically from each image by the SfM algorithm and then used to navigate the celestial body.

In this paper, we aim to achieve a complete autonomous technique for spacecraft navigation. In order to validate the proposed algorithm we use simulated images of the comet 67P/ Churyumov-Gerasimenko. The Rosetta mission to the comet 67P/Churyumov-Gerasimenko (CG) is an European Space Agency's (ESA) mission, which was launched in 2004 and rendezvoused with 67P in 2014. The Jet Propulsion Laboratory had been invited to participate in the mission and an independent orbit determination (OD) solution have been provided by the Optical Navigation (OpNav) and Orbit Determination (OD) teams [9]. Spacecraft's pose relative to the comet and comet's gravity field estimation had been operated by the Orbit Determination (OD) team at JPL. In order to pursue the spacecraft's trajectory estimation, 2-way Doppler, 2-way Range, and on-board imagery from Rosetta's NAVCAM have been used.

We state the specific assumptions of the problem and the scenario simulated as follows. First, in addition to the shape model of the small body returned by the SfM algorithm, we present how to recover the rotation, the true scale, and the center of mass of the small body along with the pose estimates of the spacecraft and the small body, providing a new estimation procedure that can be integrated by the optical navigation technique to help address the limitations of the current SPC-based optical navigation method. The rest of this paper is organized as follows. The overview of the mission and the problem statement is discussed in Section 2. Our approach to to recover the rotation of the small body, the formulation to reconstruct the pose of the camera and solve for the scale parameter by solving a nonlinear optimization problem is presented in Section 3. Simulation results are finally provided in Section 4.

2 Statement of the Problem

Rosetta is an ESA mission with the purpose of studying the comet 67P/Churyumov-Gerasimenko. The mission phase with which this paper is concern starts on August 6, 2014 and ending August 18, 2014. A total of 274 images have been acquired during this length of time. The comet navigation requires observations of recognizable surface features or

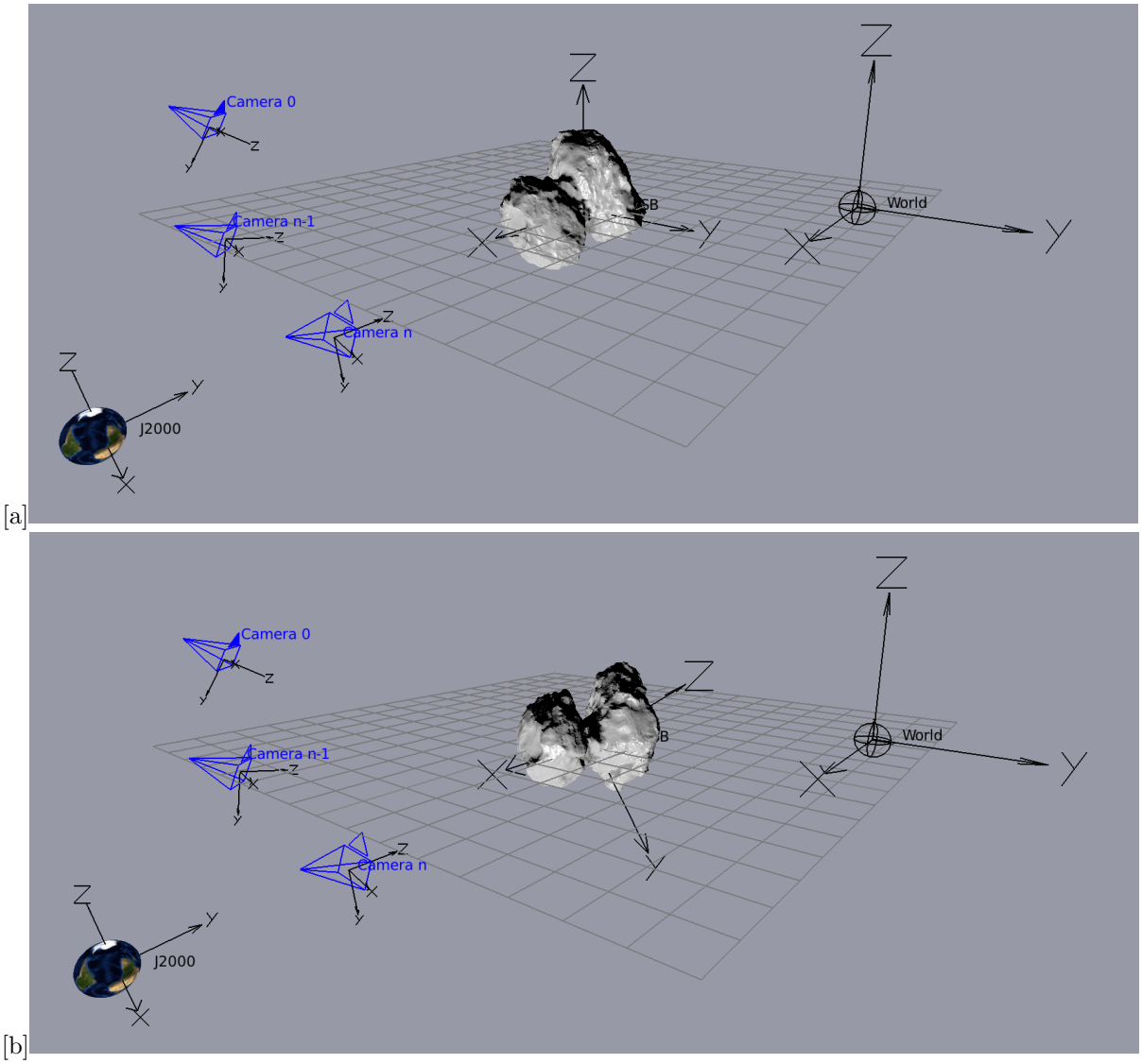

Fig. 1.2: Reference systems [a] at the first time stamp $n = 0$ and [b] at a generic time n.

landmarks to estimate the relative spacecraft's pose. The selection of landmarks points on the surface of the comet is left here to the Structure from Motion (SfM) technique [10] which autonomously estimates the relative position of the spacecraft to the small body and characterize the 3D shape of Comet 67P/Churyumov–Gerasimenko.

2.1 *Reference Frames*

The following reference frame (Figure 1.2) definition make them useful for understanding the problem:

- *Inertial Camera Frame (F_{C_0})*: An inertial camera frame centered at the first position of the camera.

- *J2000 Geocentric Earth Equatorial Inertial Frame (F_{J2000})*: The F_{J2000} frame (or called $J2000$ frame for brevity in the paper) is defined with the Earth's Mean Equator and Equinox at $12:00$ terrestrial time on January 1st, 2000. The x-axis is aligned with the mean equinox. The z-axis is aligned with the Earth's spin axis or north pole. The y-axis is rotated by $\frac{\pi}{2}$ east about the celestial equator. F_{J2000} coincides almost exactly with the International Celestial Reference System ($ICRF$) frame. No transformation is necessary to convert the F_{J2000} frame into the

$ICRF$ frame, so we treat them the same.

- *Camera Frame (F_{C_n})*: Non-inertial frame which translate and rotate with the spacecraft. The center is the perspective projection of the camera, the z-axis is parallel to the optical axis of the camera and directed to the center of the small body, and the x-axis and y-axis are perpendicular to the optical axis with x-axis pointing to the right and the y-axis pointing down.

- *World Frame (F_W)*: The non-inertial world coordinates of the reconstructed small body point cloud determined by SfM.

- *Small Body Frame (F_{SB})*: The world frame F_W shifted to the center of the small body at time 0.

For convenience, we define each frame with its own subscripts. In other words, 0 represents the inertial camera frame F_{C_0}, n the camera frame F_{C_n}, W the world frame F_W, $sb(n)$ the small body frame F_{SB} at time n, and $J2000$ the Earth-based inertial frame F_{J2000}.

2.1.1 *Simulated Images of a 3D Model*

We used `Blender` [11], an open source rendering software, to simulate the Comet 67P images. The camera locations were scripted to recreate the spacecraft's mission trajectory, as shown in Figure 2.4.

By using the time-stamps of the original images, Figure 2.1 shows some typical rendered images which can be compared to real images provided by the the spacecraft during the mission as shown in Figure 2.2. Figure 2.3 shows the trajectory of the spacecraft relative to comet 67P. The trajectory begins at a distance of about 100 km from the body and ends approximately 85 km away, following a pyramid-like trajectory in Figure 2.4.

The generated images are used as input to an open source implementation of Structure from Motion called `OpenSFM` [12, 13, 14, 15]. The `OpenSFM` code uses multiple images from different points of view to reconstruct the shape of a target object or an environment. It uses extracted and matched image keypoints in a bundle adjustment algorithm [16] to estimate the camera parameters, relative camera positions, and camera poses for every image. The underlying world frame is reconstructed under the assumption that the imaged environment is static. Using the estimated camera poses, a template matching algorithm is used to extract a dense 3D point cloud, as shown in Figure 2.5.

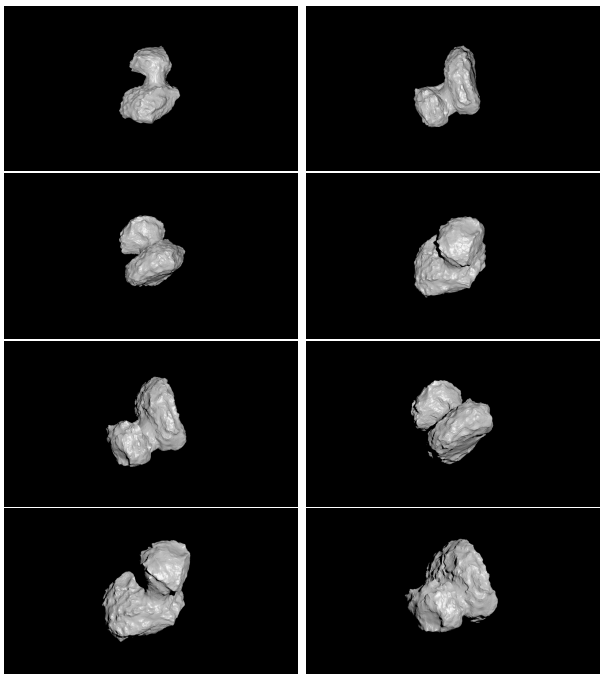

Fig. 2.1: Sequence of simulated images of the comet

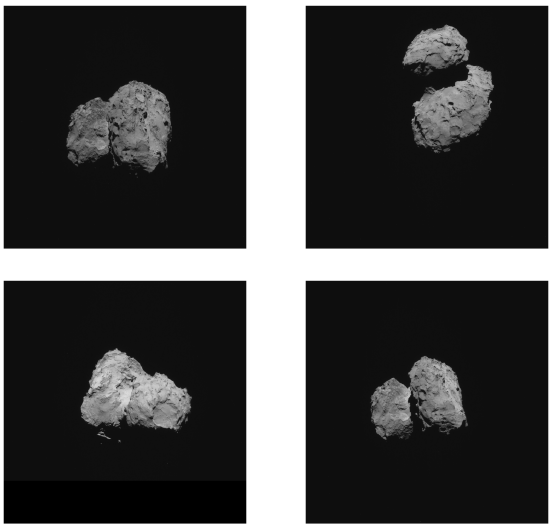

Fig. 2.2: Sequence of real images of the comet

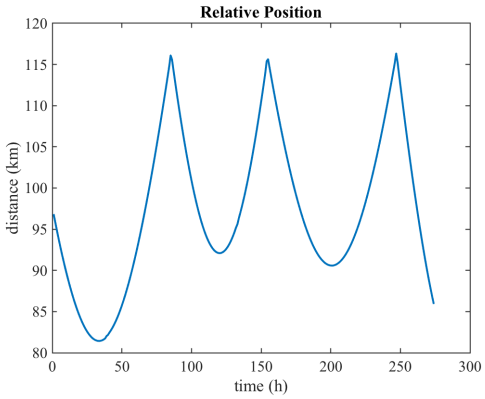

Fig. 2.3: Evolution of the cometocentric (relative to the center of a comet) distance

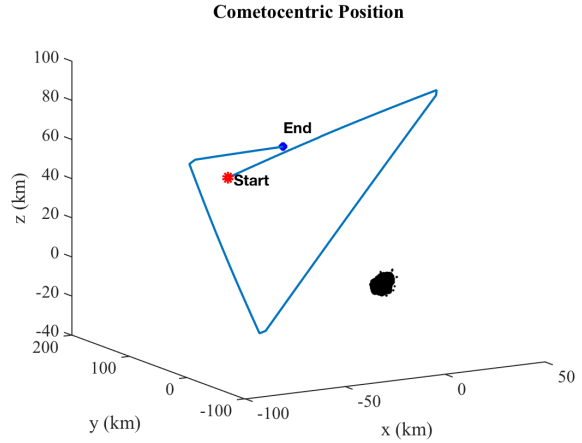

Fig. 2.4: True spacecraft trajectory of the dataset used in this paper.

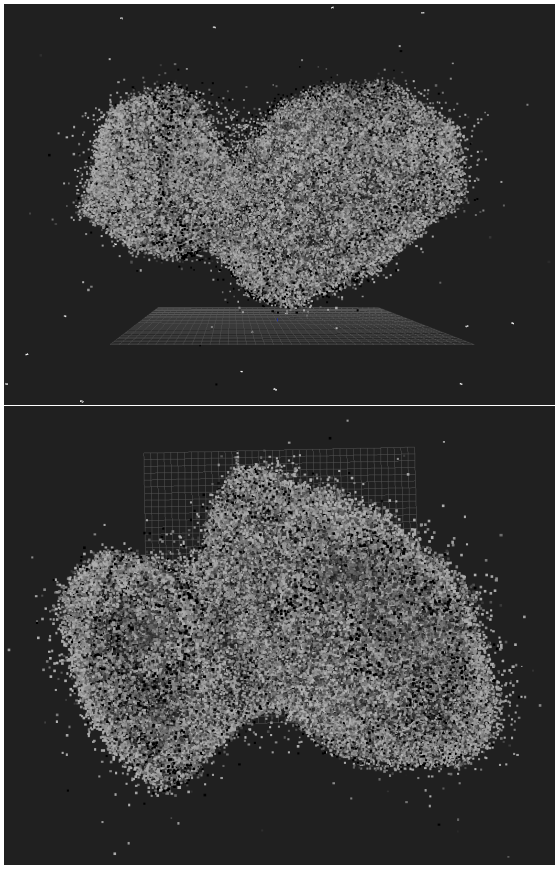

Fig. 2.5: Comet 67P points cloud obtained by the `OpenSFM` algorithm

3 Shape and Pose Estimation of a Small Body

The spacecraft is typically equipped with a monocular camera, a star tracker, and a gyroscope and it is assumed that the sensors are well calibrated and synchronized. Due to the large distance to the target, range measurements to the small body are not available at this stage. Then, Doppler range-rate measurements are used to navigate the spacecraft during the cruise phase. For our simulation, we assume that the spacecraft is controlled such that the camera is always pointing at the center of the small body such that it is within the field of view.

For each time $n = 0, 1, \ldots, N$, the navigation camera will provide time-stamped images. Processing the images in `OpenSFM` yields a rotation matrix R_n^W and a translation vector $p_{n,W}^W$ from the World Frame F_W to the camera F_{C_n} frame.

3.1 *Estimated States and Parameters*

We are interested in estimating the relative position of the spacecraft with respect to the camera F_{C_0} frame, along with the small body shape, center of gravity, and rotation matrix in the $J2000$ reference frame. Since any monocular-vision reconstruction can only recover relative positions up to a scale, we need to fuse the external distance information to also recover this parameter. Further, since the relative positions provided by our monocular reconstruction are in a static environment, we need to simultaneously recover the relative dynamics of the spacecraft and small body.

3.2 *Recovering the Small Body Rotation*

Since any rotations are scale-invariant, we can recover the small body orientation at any time with respect to the inertial $J2000$ frame by using both the orientation estimates from the SfM and the space-

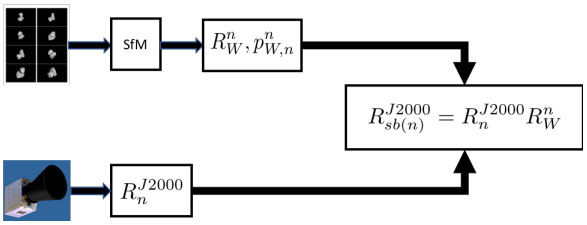

Fig. 3.1: Small body orientation recovery

craft attitude estimation from the star tracker and gyroscope, as shown in Figure 3.1. We define a new reference frame n_w, which is the camera frame at time n as seen from the non-inertial World Frame F_W, which is treated as an inertial frame in the original SfM algorithm. In contrast, F_{C_n} represents the camera frame at time n as seen from $J2000$ reference frame- the true inertial reference frame.

Consider a generic vector $v^0(0)$ in the Camera Frame F_{C_0} at time 0. The coordinates of $v^0(0)$ in the $J2000$ reference frame are given by:

$$v^{J2000}(0) = R^{J2000}_0 v^0(0). \quad [1]$$

The vector rotates with the small body and at time n it can be expressed as

$$v^{J2000}(n) = Rot_{sb(n)} v^{J2000}(0), \quad [2]$$

where $Rot_{sb(n)}$ represents the rotation of the small body in the $J2000$ frame at time n so that

$$Rot_{sb(n)} = R^{J2000}_{sb(n)} R^{sb(0)}_{J2000}. \quad [3]$$

We define $v^n(n)$ as the vector in the camera frame F_{C_n}, which gives

$$\begin{aligned} v^n(n) &= R^n_{J2000} v^{J2000}(n) \quad [4] \\ &= R^n_{J2000} R^{J2000}_{sb(n)} R^{sb(0)}_{J2000} R^{J2000}_0 v^0(0). \end{aligned}$$

Since the small body rotates in the real world, the rotation from the Camera Frame n_w to the World Frame F_W can be viewed as

$$R^W_{n_w} = R^W_{sb(n)} R^{sb(n)}_{sb(0)} R^{sb(0)}_{n_w} \quad [5]$$

The vector $v^n(n)$ as seen from the World frame can be also expressed as:

$$v^n(n) = R^n_{n_w} (R^W_{n_w})^T R^W_0 v^0(0) \quad [6]$$

where $R^n_{n_w}$ represents the rotation matrix from the camera frame n_w as seen from the World Frame W to the camera frame n (F_{C_n}) as seen from $J2000$ frame. Hence, we can now recover the rotation of the small body as follows:

$$R^{J2000}_{sb(n)} = R^{J2000}_n R^n_{n_w} R^{n_w}_W R^W_0 R^0_{J2000} R^{J2000}_{sb(0)} \quad [7]$$

where R^{J2000}_n denotes the rotation matrix from the Camera Frame at time n (F_{C_n}) to the $J2000$ frame provided by the start-tracker and gyroscope, $R^{n_w}_W$ denotes the rotation matrix returned by the SfM algorithm, and $R^n_{n_w}$ is given by Eq. (11). At time 0, the World Frame and the Small Body Frame are aligned so that $R^{sb(0)}_W = I$. The rotation matrix from the small body frame at time 0 to the $J2000$ frame is given by:

$$R^{J2000}_{sb(0)} = R^{J2000}_W = R^{J2000}_0 R^0_W \quad [8]$$

This allows us to obtain the following:

$$R^{J2000}_{sb(n)} = R^{J2000}_n R^n_W = R^{J2000}_n R^n_{n_w} R^{n_w}_{sb(0)} R^{sb(0)}_{sb(n)} R^{sb(n)}_W \quad [9]$$

The rotation matrix $R^n_{n_w}$ is unknown and has to be estimated. In this paper, the simulation has been run assuming the Z axes of the camera frame pointing to the center of the small body, the X axes to the right and the Y axis pointing down, which is the same camera frame adopted by `OpenSFM`. In this case, the rotation matrix from the camera frame defined by the SfM algorithm and the real camera frame becomes the identity matrix, $R^n_{n_w} = I$. In order to recover the rotation matrix $R^n_{n_w}$ and the translation vector p^n_{n,n_w} between the camera n_w and camera n frames, we assume that good range measurements of the spacecraft's position are available. This assumption will be relaxed for future works. Under this assumption, it is possible to retrieve the scale s, the translation vector p^n_{n,n_w}, and the rotation matrix $R^n_{n_w}$ by minimizing the error between the position of the camera ($p^n_{0,n}$) at each time n, which is provided by separate measurements, and the same position at each time n as seen from the world W frame ($R^n_{n_w} p^{n_w}_{0,n}$), returned by the SfM algorithm:

$$E_r = \left\| s(R^n_{J2000} p^{J2000}_{0,n}) - (R^n_{n_w} p^{n_w}_{0,n} + p^n_{n,n_w}) \right\|^2 \quad [10]$$

where R^n_{J2000} is from the on-board star tracker measurement at time n and $p^{J2000}_{0,n}$ is obtained by the position vector measurements between time 0 and time n from the DSN.

The first estimate of the scale s, the rotation $R^n_{n_w}$, and the translation vector p^n_{n,n_w} can be obtained by solving the following least square problem:

$$s, R^n_{n_w}, p^n_{n,n_w} = \arg \min_{s, R^n_{n_w}, p^n_{n,n_w}} \sum_n E_r \quad [11]$$

The scale estimated by Eq. (11) is then used as initial guess for the nonlinear optimization problem in section 3.3.1.

3.3 *Scale Factor and Center of Mass Trajectory Estimation*

The position of camera n in the camera coordinate frame

$$p^n_{n,n} = R^n_W p^W_{n,W} + p^n_{W,n}. \quad [12]$$

can be expressed as $p^W_{n,W}$ in the World coordinate frame:

$$p^W_{n,W} = R^W_n (p^n_{n,n} - p^n_{W,n}) = -R^W_n (p^n_{W,n}). \quad [13]$$

Let $p^{sb(0)}_{n,sb(0)}$ denote the position vector of the camera at time n relative to the origin of the small body at time 0, called $sb(0)$ in the small body frame. Consequently, the position of the camera at time n relative to the small body at time 0 is

$$p^{sb(0)}_{n,sb(0)} = p^W_{n,W} - p^W_{sb(0),W} \quad [14]$$

where $p^W_{n,W}$ is given in Eq. (13), and $R^{sb(0)}_W = I$ is used to simplify the equation since the World Frame W is aligned with the $sb(0)$ frame. Also, let $p^W_{n,W}$ denote the position of the camera n in W and $p^W_{sb(0),W}$ the position of the CM of the small body in the world frame W. The scaled position of the camera n relative to $sb(0)$ in the $J2000$ reference frame is

$$s(p^{J2000}_{n,sb(0)}) = R^{J2000}_0 R^0_{sb(0)} p^{sb(0)}_{n,sb(0)} \quad [15]$$

where the constant s denotes the unknown scaling factor. At time n it becomes

$$s(p^{J2000}_{n,sb}) = Rot_{sb} s(p^{J2000}_{n,sb(0)}) \quad [16]$$

where $Rot_{sb(n)}$ is defined in Eq. (3) as:

$$Rot_{sb} = R^{J2000}_{sb(n)} (R^{J2000}_{sb(0)})^T \quad [17]$$

Then, the position of the camera n in the small body reference frame at time n can be written as

$$\begin{aligned} & p^{sb}_{n,sb} \quad [18] \\ & = R^{sb}_0 R^0_{J2000} R^{J2000}_{sb} R^{sb(0)}_{J2000} R^0_0 R^{J2000}_{sb(0)} p^{sb(0)}_{n,sb(0)} \\ & = R^{sb}_0 R^0_{J2000} R^{J2000}_{sb} p^{sb(0)}_{n,sb(0)} \end{aligned}$$

We are interested in finding the position of the camera n in the world frame W (i.e., $p^W_{n,W}$). In order to obtain it, we need to add the CM position of the small body at time n (i.e., $p^W_{sb,W}$) to the position of the camera n in the small body frame at time n (i.e., $p^W_{n,sb}$):

$$p^W_{n,W} = R^W_{sb} p^{sb}_{n,sb}(n) + p^W_{sb,W} \quad [19]$$

Then, the position of the camera n with respect to the camera 0 frame can be expressed as

$$\begin{aligned} p^0_{n,0} &= R^0_W p^W_{n,W} + p^0_{W,0} \quad [20] \\ &= R^0_W (R^W_{sb} p^{sb}_{n,sb}(n) + p^W_{sb,W}) + p^0_{W,0} \\ &= R^0_W (R^W_0 R^0_{J2000} R^{J2000}_{sb(n)} p^{sb(0)}_{n,sb(0)} + p^W_{sb,W}) + p^0_{W,0} \\ &= R^0_W [S_n p^{sb(0)}_{n,sb(0)} + p^W_{sb(n),W}] + p^0_{W,0} \\ &= R^0_W S_n p^{sb(0)}_{n,sb(0)} + R^0_W p^W_{sb(n),W} + p^0_{W,0} \\ &= R^0_W S_n (p^W_{n,W} - p^W_{sb(n),W}) + R^0_W p^W_{sb(n),W} + p^0_{W,0} \\ &= R^0_W (I - S_n) p^W_{sb(n),W} + R^0_W S_n p^W_{n,W} + p^0_{W,0} \\ &= R^0_W (I - S_n) p^W_{sb(n),W} + D_n \\ &= E_n p^W_{sb(n),W} + D_n \end{aligned}$$

where $S_n = R^W_0 R^0_{J2000} R^{J2000}_{sb(n)} = R^W_{sb(n)}$, $D_n = R^0_W S_n p^W_{n,W} + p^0_{W,0}$, and $E_n = R^0_W (I - S_n)$. Also, we used $R^{sb(0)}_W = I$.

3.3.1 *Nonlinear Optimization*

Given the position of the camera in the F_{C_0} reference frame at time n, we want to estimate the scale and the small body center of gravity by minimizing the error over all of the estimated camera positions. By using Eq. (20), the error of the camera position is given as

$$\begin{aligned} E_{p_n} &= \left\| p^0_{n,0} - s(R^0_{J2000} p^{J2000}_{n,0}) \right\|^2 \quad [21] \\ &= \left\| E_n p^W_{sb(n),W} + D_n - s(R^0_{J2000} p^{J2000}_{n,0}) \right\|^2 \end{aligned}$$

where $p^{J2000}_{n,0}$ denotes the true position of the camera provided by the DSN antenna. The error between the center of rotation of the small body and the centroid of the small body returned by the SfM algorithm is given as

$$E_{c_n} = \left\| p^W_{sb,W} - Cn^W_{sb} \right\|^2 \quad [22]$$

where Cn^W_{sb} the centroid of the small body obtained from the points clouds returned from the SfM algorithm. Then, we can solve for the scale and the CM of the small body as follows:

$$s, p^W_{sb,W} = \arg \min_{s, p^W_{sb,W}} \left(\sum_n E_{p_n} + \sum_n E_{c_n} \right) \quad [23]$$

$$= \arg \min_{s, p^W_{sb,W}} \left(\sum_n \left\| E_n p^W_{sb,W} + D_n - s(R^0_{J2000} p^{J2000}_{n,0}) \right)^2 + \sum_n \left\| p^W_{sb,W} - C n^W_{sb} \right\|^2 \right)$$

Note that the position data from the DSN ($R^0_{J2000} p^{J2000}_{n,0}$) can be replaced by some predicted position measurements based on the initial position measurement and the velocity estimate (e.g., from the DSN). Also, once Lidar or radar measurements become available, such direct depth measurements can be used to improve the accuracy of the monocular-vision-based estimation method used in this paper. Furthermore, if the spacecraft enters the strong gravity-well region of the small body, the relative orbital dynamics between the small body and the spacecraft can be used to provide additional information to the optimization problem in Eq. (23).

4 Simulation Results

In this section, the proposed approach to estimate the scale and CM of the small body is implemented. We present here some preliminary simulation results. First, we make the assumption that accurate information of the spacecraft trajectory are available. Subsequently, we relax this assumption by considering uncertainties in the provided data.

4.1 *Estimation of Attitude Trajectories of the Small Body*

The Euler angles recovered from the estimated rotation matrix of the small body, $R^{J2000}_{sb(n)} in$ Eq. (9), are compared with the truth values of the small body Euler angles, as shown in Fig. 4.1. The true data has an initial Euler angle rate of $66,3°$ for the right ascension (RA), $65,2°$ for the declination angle (Dec) and $284.1°$ for the Prime Meridian (PM), which are converted into radiant at the beginning of the simulations. The true rotation matrix from the inertial $J2000$ frame to the small body frame is given by:

$$R^{sb(n)}_{J2000} = R_z(PM) R_x(\frac{\pi}{2} - Dec) R_z(RA) \qquad [24]$$

The first row of Fig. 4.1 shows continuous spinning motion about the Z axis (Ψ) of the small body Comet 67P (clockwise or negative rotation), as seen in the decreasing value from $+\pi$ to $-\pi$. The Θ and Φ values of Fig. 4.1 show bounded oscillatory motions at a rate of 0.47 rad/s, which is consistent with the known principal-axis rotation period of 12.40 hours.

Figure 4.2 shows the error between the true and estimated values of the Euler angles of the small body. The errors of the Φ and Θ angles effectively remained effectively well within the bound of $\pm$ 0.05 radians, while the Ψ rotation error stayed within the bound of $\pm$ 0.3 radians. These numbers can be further improved using more data points.

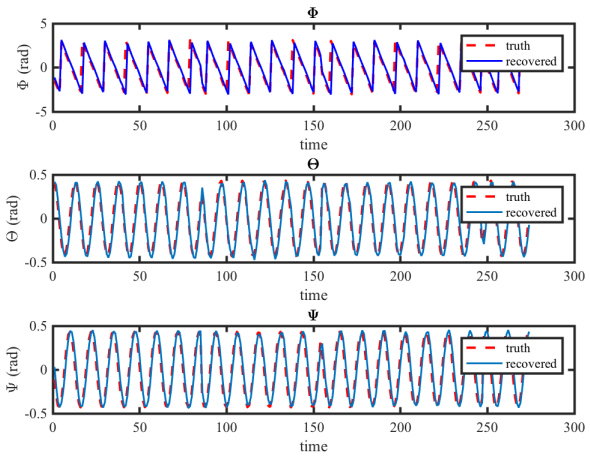

Fig. 4.1: Estimated angles (rad) vs truth data (rad).

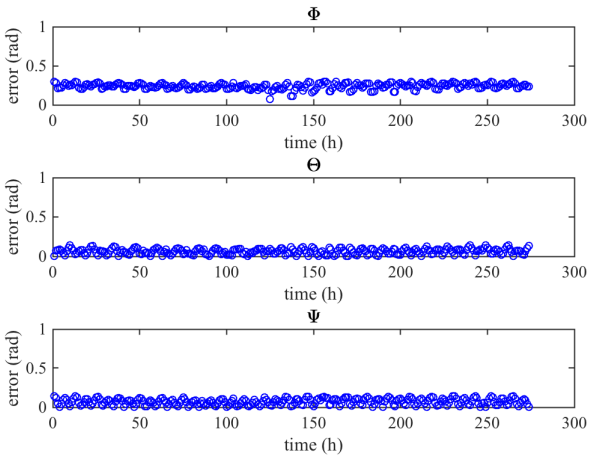

Fig. 4.2: Error between the Euler angles estimated and the true values.

4.2 *Noise-Free Trajectory Estimation*

We assume that accurate information of the spacecraft position is provided by the 2-way Doppler and range measurements. Figures 2.3 and 2.4 show the simulated trajectory of the spacecraft.

The true trajectory of the spacecraft is rotated and translated from the $J2000$ reference frame into

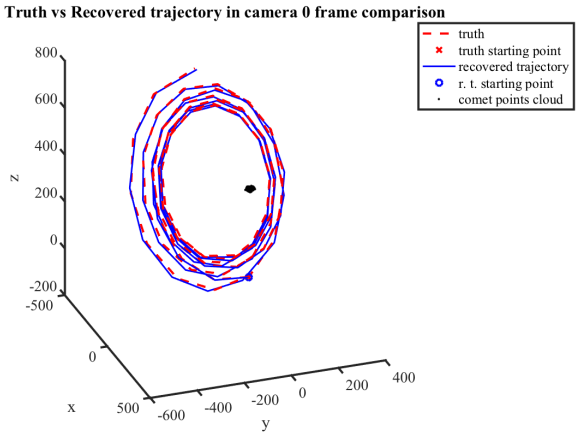

Fig. 4.3: Scale and trajectory recovery with noise-free measurements (plotted in camera 0 frame).

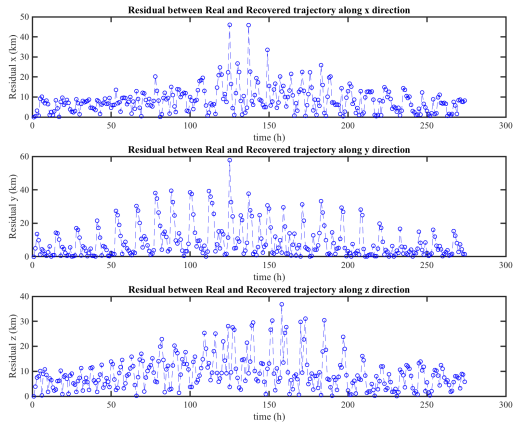

Fig. 4.4: Error between the truth and the estimated trajectory with noise-free measurements.

the camera 0 reference frame and compared with the estimated trajectory $p^0_{n,0}$. The scale factor estimated by solving Eq. (23) is applied to the truth and the resulting trajectory is then compared with the estimated one in Figure 4.3, where the dashed red line represents the truth trajectory and the blue one is the estimated trajectory. The value of the estimated scale factor that minimize the nonlinear least square in Eq. (14) is 4.3507.

Figure 4.4 shows the spacecraft position estimation error of the true data versus the estimated one along both the x, y, and z directions.

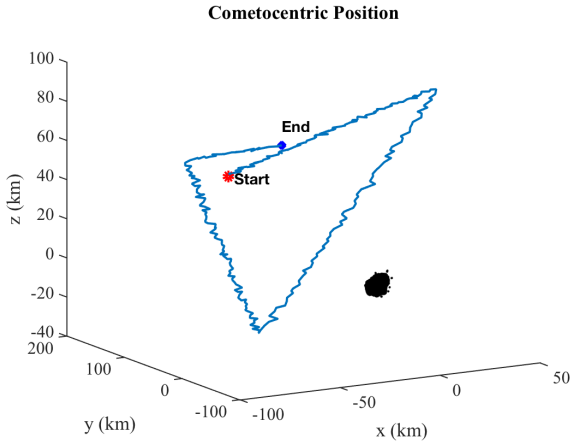

Fig. 4.5: Spacecraft trajectory measured with random noise.

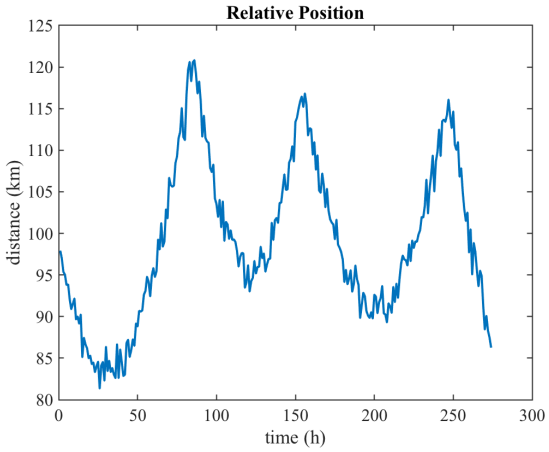

Fig. 4.6: Evolution of the cometocentric distance with random noise.

4.3 *Trajectory Estimation with Noisy and Inaccurate Measurements*

In a real situation, spacecraft position measurements are not accurate. In order to test the algorithm in more realistic scenario we make here the assumption that we have an uncertainty of 5 km in the position measurements. In order to obtain it we introduced a Gaussian noise with zero mean and variance σ=5 km. The new spacecraft trajectory which is used in the simulation is shown in Figures 4.5 and 4.6. The value of the scale estimated by solving Eq. (23) is 4.3596. Figure 4.7 compares the new estimated trajectory against the true data, while their error is shown in Figure 4.8.

From Figure 4.4 and 4.8 we can see that the error

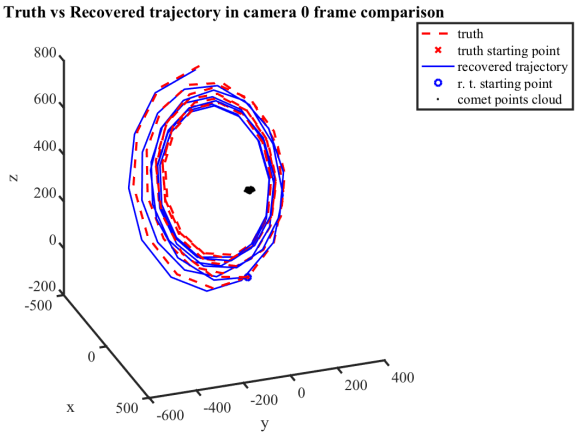

Fig. 4.7: Scale recovery with measurement errors of spacecraft position (plotted in camera 0 frame).

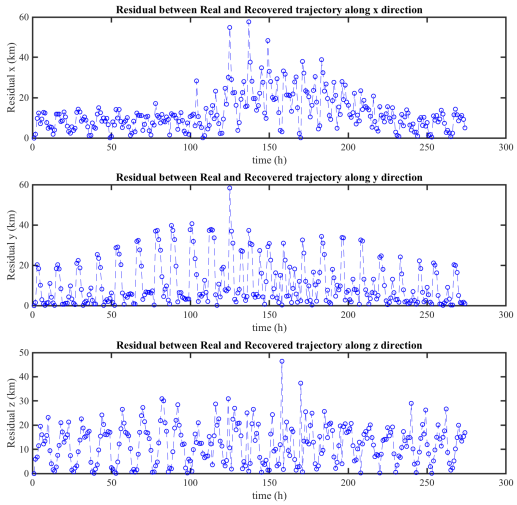

Fig. 4.8: Error between truth and estimated trajectory with noisy spacecraft position measurements.

between the estimated trajectory and the true data has a mean value of about 10 km in the case of using precise spacecraft pose measurements and approximately 15-20 km if noisy spacecraft pose measurements are used. If the distance between the comet and the spacecraft is close enough to allow for Lidar or radar measurements, such measurement can dramatically improve the accuracy of the proposed algorithm.

From these results, we can also find that the proposed feature-based SfM algorithm can perform the scale recovering quite accurately even in the presence of measurement noise. However, Figures 4.4 and 4.8 present a large amount of scattering between two consecutive data position. Further investigations will focus on understanding the reason of this scattering and how to reduce the residual error between the two trajectories.

5 Conclusion

The navigation systems for small body exploration missions have relied on extensive use of on-ground resources on Earth. In this paper, we have presented a vision-based estimation algorithm for autonomous navigation and real-time construction of a small body shape that would provide an important step toward enabling a complete autonomous approach of small bodies. The proposed optimization-based estimation algorithm for autonomous optical navigation would enable the spacecraft to autonomously approach and maneuver around an unknown small body by mapping its geometric shape, estimating its orientation, and simultaneously determining the spacecraft's orbit, thereby helping to reduce the reliance on ground-in-the-loop operations. In contrast with the existing method of Stereo Photoclinometry that uses pixel-based mapping, the proposed method combines feature-based Structure from Motion (SfM) techniques and real-time optimization that employ sequential updates and computational acceleration enhancements with other sensor measurements, yielding orientation and position estimates with scale recovery of both spacecraft and a small body. Note that the results in this paper are obtained by assuming a complete knowledge of the spacecraft trajectory, based on a reconstruction derived by a combination of Doppler and range measurements along with the SPC technique. Hence, the information came strictly as a measurement from the DSN, i.e. as a post-processed result. Future work will focus on relaxing the assumption that spacecraft position information is provided by radiometric tracking measurements from Earth, along with improving real-time computational performance of the algorithm, and the use of dynamics constraints for proximity approach.

Acknowledgement

This work was supported by the Jet Propulsion Laboratory (JPL). Government sponsorship is acknowledged. This research was carried out in part at the JPL, California Institute of Technology, under

a contract with NASA. The authors thank Saptarshi Bandyopadhyay and Nick Mastrodemos.

References

[1] R. W. Gaskell, O. S. Barnouin-Jha, D. J. Scheeres, A. S. Konopliv, T. Mukai, S. Abe, J. Saito, M. Ishiguro, T. Kubota, T. Hashimoto, et al. Characterizing and navigating small bodies with imaging data. *Meteoritics & Planetary Science*, 43(6):1049–1061, 2008.

[2] B. Godard, F. Budnik, P. Muñoz, T. Morley, and V. Janarthanan. Orbit determination of Rosetta around comet 67P Churyumov-Gerasimenko. In *Proceedings 25th International Symposium on Space Flight Dynamics–25th ISSFD, Munich, Germany*, 2015.

[3] R Pardo de Santayana, M Lauer, P Muñoz, and F Castellini. Surface characterization and optical navigation at the Rosetta flyby of asteroid Lutetia. In *International Symposium on Space Flight Dynamics*, 2014.

[4] C. Olson, R. P. Russell, and S. Bhaskaran. Spin State Estimation of Tumbling Small Bodies. *The Journal of the Astronautical Sciences*, 63(2):124–157, 6 2016.

[5] W. M. Owen Jr. Methods of optical navigation. AAS/AIAA Space Flight Mechanics Meeting,American Astronautical Soc. Paper 2011-215,2011,Pasadena, CA: Jet Propulsion Laboratory, National Aeronautics and Space Administration.

[6] S. Bhaskaran, S. Nandi, S. Broschart, M. Wallace, L. A. Cangahuala, and C. Olson. Small body landings using autonomous onboard optical navigation. *The Journal of the Astronautical Sciences*, 58(3):409–427, 2011.

[7] K. Meier, S.-J. Chung, and S. Hutchinson. Visual-inertial curve simultaneous localization and mapping: Creating a sparse structured world without feature points. *Journal of Field Robotics*, 35(4):516–544, 2018.

[8] J. Yang, A. Dani, S.-J. Chung, and S. Hutchinson. Vision-based localization and robot-centric mapping in riverine environments. *Journal of Field Robotics*, 34(3):429–450, 2017.

[9] Stephen Broschart, Shyam Bhaskaran, Julie Bellerose, Ann Dietrich, Dongsuk Han, Robert Haw, Nickolaos Mastrodemos, William M Owen, Brian Rush, and David Surovik. Shadow navigation support at JPL for the Rosetta landing on comet 67P/Churyumov-Gerasimenko. In *26th International Symposium on Space Flight Dynamics ISSFD, number ISSFD-2017-096*, 2017.

[10] O. Özyeşil, V. Voroninski, R. Basri, and A. Singer. A survey of structure from motion*. *Acta Numerica*, 26:305–364, 2017.

[11] R. Hess. *The essential Blender: guide to 3D creation with the open source suite Blender*. No Starch Press, 2007.

[12] P. F. Alcantarilla and T. Solutions. Fast explicit diffusion for accelerated features in nonlinear scale spaces. *IEEE Trans. Patt. Anal. Mach. Intell*, 34(7):1281–1298, 2011.

[13] P. F. Alcantarilla, A. Bartoli, and A. J. Davison. KAZE features. In *European Conference on Computer Vision*, pages 214–227. Springer, 2012.

[14] R. Hartley and A. Zisserman. *Multiple view geometry in computer vision*. Cambridge university press, 2003.

[15] H Christopher Longuet-Higgins. A computer algorithm for reconstructing a scene from two projections. *Nature*, 293(5828):133, 1981.

[16] B. Triggs, P. F. McLauchlan, R. I. Hartley, and A. W. Fitzgibbon. Bundle adjustment—a modern synthesis. In *International workshop on vision algorithms*, pages 298–372, 1999.